



Co_xNi_y-decorated graphene as novel, stable and super effective non-precious electro-catalyst for methanol oxidation



Nasser A.M. Barakat^{a,b,*}, Moaaed Motlak^c

^a Organic Materials and Fiber Engineering Department, Chonbuk National University, Jeonju 561-756, Republic of Korea

^b Chemical Engineering Department, Minia University, El-Minia, Egypt

^c Department of Physics, College of Science, Anbar University, Anbar 31001, Iraq

ARTICLE INFO

Article history:

Received 30 October 2013

Received in revised form 12 January 2014

Accepted 11 February 2014

Available online 19 February 2014

Keywords:

Graphene

Methanol electrooxidation

Non-precious electrocatalyst

DMFCs

CoNi alloy

ABSTRACT

Graphene and alloy structure can overcome the main problem facing the non-precious electro-catalysts; low performance and poor stability. In this study, Co_xNi_y-decorated graphene is introduced as novel, super effective and stable non-precious electro-catalyst for methanol oxidation. The obtained results have indicated that utilizing graphene as a support strongly enhances the electro-catalytic activity as the current density was doubled ten times, moreover a negative onset potential (−40 mV vs. Ag/AgCl) was obtained which is a distinct progress in the non-precious electro-catalysts research field. The electronic structure which is controlled by the alloy composition showed strong influence on the electro-catalytic activity; Co_{0.2}Ni_{0.2} alloy nanoparticles revealed the best performance while Co_{0.1}Ni_{0.3} nanoparticles were the worst. Due to the alloy structure, the introduced graphene-supported electro-catalyst reveals distinguished stability. In-situ decoration of graphene by Co_xNi_y alloy nanoparticle is utilized to produce the introduced electro-catalyst. Briefly, cobalt acetate and nickel acetate were added to the reaction media during graphene preparation using a modified chemical route. Later on, the resultant material was calcined in argon atmosphere at 850 °C. The utilized physicochemical characteristics affirmed formation of multi-layer graphene sheets decorated by solid solution Co_xNi_y alloy nanoparticle.

© 2014 Elsevier B.V. All rights reserved.

1. Introduction

Depletion of the fossil energy sources forces the researchers worldwide to seek about convenient alternatives. Because of the simple system structure, low cost of fuels, and easiness of fuel handling compare to hydrogen gas, direct alcohol fuel cells (DAFCs) are very attractive electricity generating system [1]. Moreover, DAFCs have shown that they can produce higher current densities than proton exchange membrane fuel cells (PEMFCs) [2].

Among the introduced DAFCs, direct methanol fuel cells (DMFCs) have received much attention during the last decade [3], because methanol is an inexpensive, readily available, and easily stored and transported liquid fuel. DMFCs do not have many of the fuel storage problems typical of some fuel cells because methanol has a higher energy density than hydrogen—though less than gasoline or diesel fuel. Methanol is also easier to supply to the public

using our current infrastructure. In the DMFCs, methanol is directly oxidized at the anode to produce carbon dioxide and water, providing a new way to store and convey the energy [4,5]. The anodic reactions in the DMFCs are considered to be a combination of adsorption and electrochemical reaction on the anode surface [6,7]. Accordingly, because of the adsorption capacity, carbon has been incorporated in many recently reported electro-catalytic materials [8–12].

As a novel carbonaceous material, graphene has attracted great attentions due to its marvelous physicochemical characteristics [13]. Remarkably, graphene is the thinnest and strongest material reported so far, exhibiting outstanding properties such as excellent conductance of both heat and electricity, and being the strongest material ever measured properties [14]. In this regard, electrons move through graphene as if they have no mass. Single-layer graphene is predicted to have a large surface area close to 2600 m²/g [15] which strongly enhances the adsorption capacity. As a consequence, graphene has been the subject of more research papers and patent applications reported in science in the last few years [16].

Currently, almost all pre-commercial low-temperature fuel cells use Pt-based electro-catalysts [17,18]. Graphene-Pt composites showed very good performance [19–23]. Unfortunately, beside the

* Corresponding author at: Organic Materials and Fiber Engineering Department, Chonbuk National University, Jeonju 561-756, Republic of Korea.
Tel.: +82 632702363; fax: +82 632702348.

E-mail address: nasser@jbnu.ac.kr (N.A.M. Barakat).

high capital cost, the catalyst poisoning by CO or CHO species is another real problem facing most of the Pt-based electro-catalysts [5,24,25].

Poor chemical stability and low electro-catalytic activity are the main problems against commercial applications of the transition metals. Among the transition metals, nickel is commonly used as an electro-catalyst for both anodic and cathodic reactions in many applications [26–28]. However, pristine nickel suffers from the aforementioned problems. The study of alloy electrodes is motivated primarily from the anticipation of a synergistic electro-catalytic benefit from the combined properties of the alloys components. Moreover, a promising characteristic of such alloy electrodes is the resistance to corrosion in the alkaline media. Accordingly, Ni-based alloys were investigated as electro-catalysts for DAFCs [29–32]. Although cobalt was not introduced as a sole electro-catalyst due to its low electro-catalytic activity, it was used as a co-catalyst to annihilate the Pt poisoning [33] which enhances the performance.

In this study, Co_xNi_y -decorated graphene is introduced as effective and stable catalyst for methanol electro-oxidation. The introduced electro-catalyst was prepared based on a modified Hummer's method [34,35]. Full study including the influence of the metallic nanoparticles and their loading was achieved. The results emphasized the priority of graphene and alloy structure in enhancing the electro-catalytic activity and chemical stability, respectively.

2. Experimental

2.1. Materials

Cobalt (II) acetate tetra-hydrate (CoAc, 98% assay Junsei Chemical Co., Ltd, Japan), and nickel acetate tetrahydrate (NiAc, 99.0% assay, Sigma–Aldrich) without any further modification were utilized as metals precursors. However, graphene was synthesized using graphite powder (<20 μm), hydrogen peroxide, hydrazine monohydrate and sulphuric acid (95–97%) which were purchased from Sigma–Aldrich.

2.2. Procedures

2.2.1. Preparation of graphene oxide (GO)

Graphene was prepared chemically from reduction of exfoliated graphene oxide (GO) which was synthesized from natural graphite powder by a modified Hummer's method [34]. First, five grams graphite treated twice by 5% HCl was placed in cold concentrated H_2SO_4 (130 ml), then 15 g of KMnO_4 was added gradually to the mixture in the ice bath with stirring for 2 h. The system was diluted with DI water and then the temperature was increased to 98 °C. Later on, the mixture was cold to room temperature then H_2O_2 (50 ml, 30 wt%) was added, the mixture was left overnight. The mixture was filtered under vacuum and washed with 10% aqueous HCl several times. Then, the filter cake was washed several times using distilled water to remove any acid, the washing was utilized until getting neutral filtrate (pH ~ 7). Finally, the obtained powder was dried under vacuum at 50 °C over night,

2.2.2. Preparation of CoNi-loaded graphene

It is noteworthy mentioning that in all experiments, the utilized amount from GO was 300 mg. In 250 ml round flask, GO powder were dispersed in 400 ml distilled water and ultrasonicated for 40 min then 0.5 ml of hydrazine hydrate was added to the suspended GO. Specific amounts from CoAc and NiAc were dissolved individually in the minimum amounts of water and mixed with the GO suspension. Typically, to study the loading weight, 0.1, 0.2

and 0.4 g from each salt was utilized. However, to study the influence of the metallic nanoparticles composition, the loading weight was fixed at 0.4 g (total salts), the utilized NiAc:CoAc amounts (g:g) were 0.0:0.4, 0.1:0.3, 0.2:0.2, and 0.4:0.0. The slurry was refluxed at 150 °C for 10 h. Then, the solution was filtered. The obtained filter cake was washed several times by plenty amounts of water, dried under vacuum at 80 °C for one night, and then calcined under argon atmosphere at 850 °C for 2 h.

2.3. Characterization

Rigaku X-ray diffractometer (XRD, Rigaku, Japan) with Cu K α ($\lambda = 1.5406 \text{ \AA}$) radiation over Bragg angle ranging from 10° to 100° was invoked to have information about the phase and crystallinity. Transmission electron microscope (TEM, JEOL JEM-2010, Japan) operated at 200 kV equipped with EDX analysis was utilized to get normal and high resolution images. Nanofinder 30 spectrometer (Tokyo Inst. Co., Japan) equipped with a He:Ne ($\lambda = 633 \text{ nm}$ laser) was utilized to check the Raman spectra, the scattering peaks were calibrated with a reference peak from a Si wafer (520 cm^{-1}). The spectra were recorded under a microscope with a 40 \times objective in range of 0–1600 cm^{-1} and 3 mW of power at the sample. VersaSTAT 4 (USA) electrochemical analyzer and a conventional three-electrode electrochemical cell were utilized to investigate the electrochemical measurements. A Pt wire and an Ag/AgCl electrode were used as the auxiliary and reference electrodes, respectively. Glassy carbon electrode was used as working electrode. Preparation of the working electrode was carried out by mixing 2 mg of the functional material, 20 μl Nafion solution (5 wt%) and 400 μl isopropanol. The slurry was sonicated for 30 min at room temperature. 15 μl from the prepared slurry was poured on the active area of the glassy carbon electrode which was then subjected to drying process at 80 °C for 20 min. Normalization of the obtained current densities were performed based on the surface area of the utilized glassy carbon electrodes (0.07 cm^2).

3. Results and discussion

Chemical reduction of GO process provides not only an established, low-cost and scalable approach for graphene preparation, but also a highly flexible method for the chemical functionalization of graphene materials [36,37]. GO readily forms stable colloidal suspensions of thin sheets in water due to the hydrophilic nature of the oxygenated graphene layers [38]. After a suitable ultrasonic treatment, such exfoliation can produce stable dispersions of very thin graphene oxide sheets in water [36]. Easy and trustable differentiation between graphite, GO and graphene can be carried out by using XRD analysis. For instance, the graphitic structure is assigned by a sharp peak at 2θ of 26.5° ((002) crystal plan) [39]. After oxidation to GO, a new diffraction peak appears at 2θ of 10.5°, along with the disappearance of the graphite peak [39]. However, graphene is identified by a broaden peak at 2θ of 27.5° [35,40] which indicates small crystalline size of graphene in single or few layers structure. Accordingly, from Fig. 1A which represents the XRD pattern of the prepared graphene, one can claim that the obtained powder composes of graphene that indicates that the chemical procedure for graphene preparation has been successfully achieved. Fig. S1 in the supporting information displays the XRD patterns of the utilized graphite, GO and the produced graphene.

Beside XRD, Raman microscopy can also provide a trustable comparison between graphite, GO and graphene. For instance, graphite displays a prominent G peak at 1581 cm^{-1} , corresponding to the first-order scattering of the E_{2g} mode [41]. However, in the Raman spectrum of GO, the G band is broadened and shifted to 1594 cm^{-1} . Moreover, because of the reduction in size of the

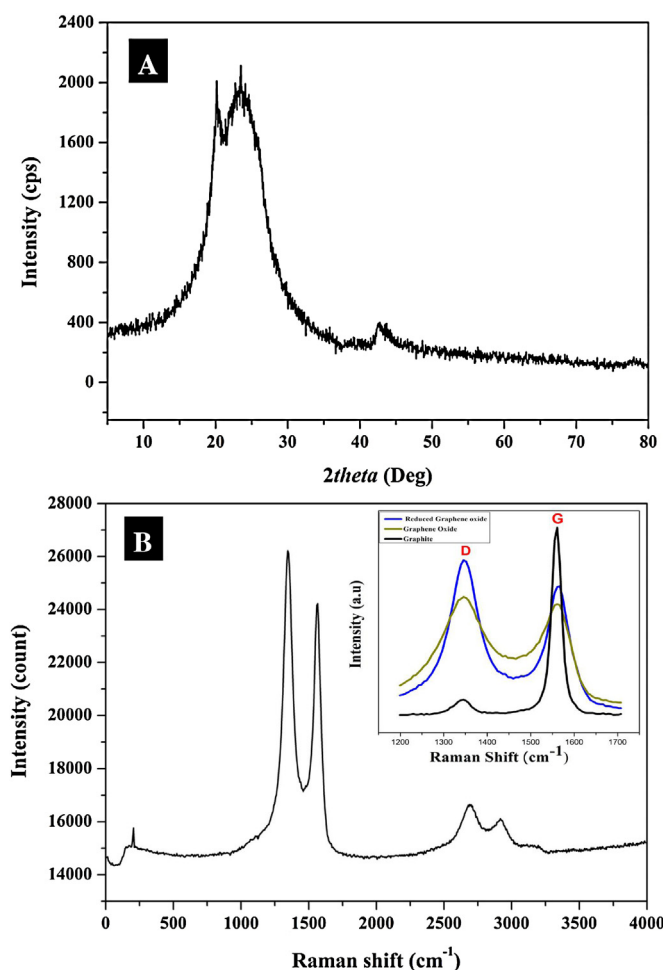


Fig. 1. XRD; (A), and Raman spectroscopy; (B) analyses for the prepared graphene. The inset in panel B displays the D and B peaks in the utilized graphite, GO and reduced GO..

in-plane sp² domains due to the extensive oxidation, the D band at 1363 cm⁻¹ becomes prominent. On the other hand, the Raman spectrum corresponding to graphene contains both G and D bands (at ~1580 and ~1350 cm⁻¹, respectively) with an increase in the D/G intensities ratio compared to that in GO. This change suggests a decrease in the average size of the sp² domains upon reduction of the exfoliated GO [41]. Fig. 1B displays the Raman spectrum of the prepared reduced graphene oxide. As shown in the figure, the pattern typically matches the standard graphene. Fig. S.2 in the supporting information represents Raman spectra utilized graphite, GO and the produced graphene.

Fig. 2 represents the TEM image for the prepared graphene, as shown the exfoliation clearly appears. Moreover, the corresponding inset displays the HR TEM indicates that the formed graphene is multilayer; around 3 layers. From XRD, Raman and TEM analyses, it can be confirmed that the utilized procedure was successfully achieved to produce graphene.

Fig. 3 displays the XRD analysis of the sintered powder obtained after addition of the metals acetates during graphene preparation. The strong diffraction peaks at 2θ values of 44.30°, 51.55°, 76.05° and 92.55° corresponding to (1 1 1), (2 0 0), (2 2 0) and (3 1 1) crystal planes, respectively indicate the formation of pure nickel or pure cobalt or both (JCDPS 15-0806; Co and 04-0850; Ni). Cobalt and nickel have successive atomic numbers, close molecular weights, and same crystal structure in the normal conditions; they have FCC crystal lattice with space group class (S.G) of Fm3m(225). The cell parameters are 3.544 and 3.523 Å for the cobalt and nickel,

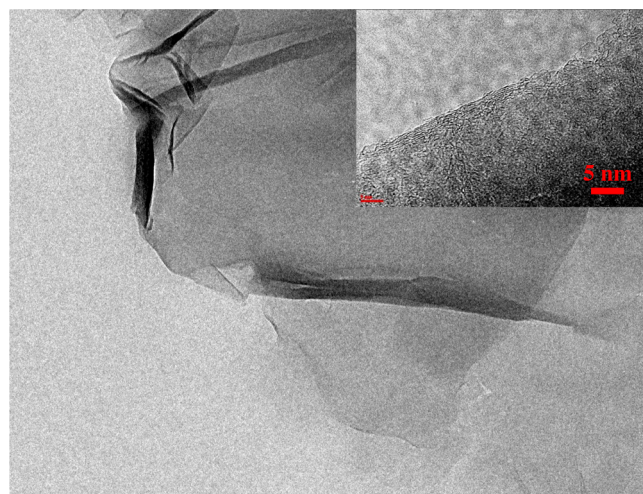


Fig. 2. TEM and HR TEM (inset) of the prepared graphene..

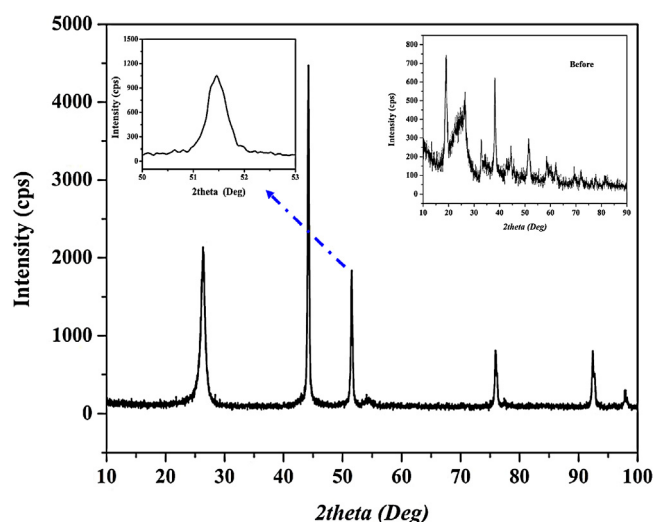


Fig. 3. XRD results for the prepared docrated graphene after and before (inset) calcination. The second inset represents the (200) peak..

respectively. Accordingly, the XRD spectra of Ni and Co are almost similar. In fact, XRD can provide important information about whether Ni and Co are present separately or in the form of an alloy structure. The little differences in the cell parameters, 3.544 Å of cobalt and 3.523 Å of Ni should have the (2 0 0) peak at 51.53° and 51.86°, respectively. A single peak within that range would indicate formation of a solid solution. As shown in the left inset (Fig. 3) which displays the (200) peak, single peak was obtained which indicates formation of CoNi solid solution. It is noteworthy mentioning that, upon addition of the metallic precursors to GO suspension, the utilized reducing agents could not achieve complete reduction for the utilized metal precursors. XRD analysis for the precipitate obtained after the reflux step indicates that the metallic counterpart composed of Co(OH)₂ (JCDPS # 45-0031) and Ni(OH)₂ (JCDPS # 14-0117) (the right inset in Fig. 3).

TEM analyses were carried out to further investigate the real composition of the formed metallic compounds and the obtained morphology (Fig. 4). Fig. 4A displays the normal TEM image, as shown dark spots from crystalline nanoparticles are distributed along the graphene sheet. Co and Ni distributions were investigated by performing elemental analysis along with randomly chosen lines (Fig. 4B–D). As shown, Co and Ni have the same distribution along with the chosen lines that verifies the aforementioned

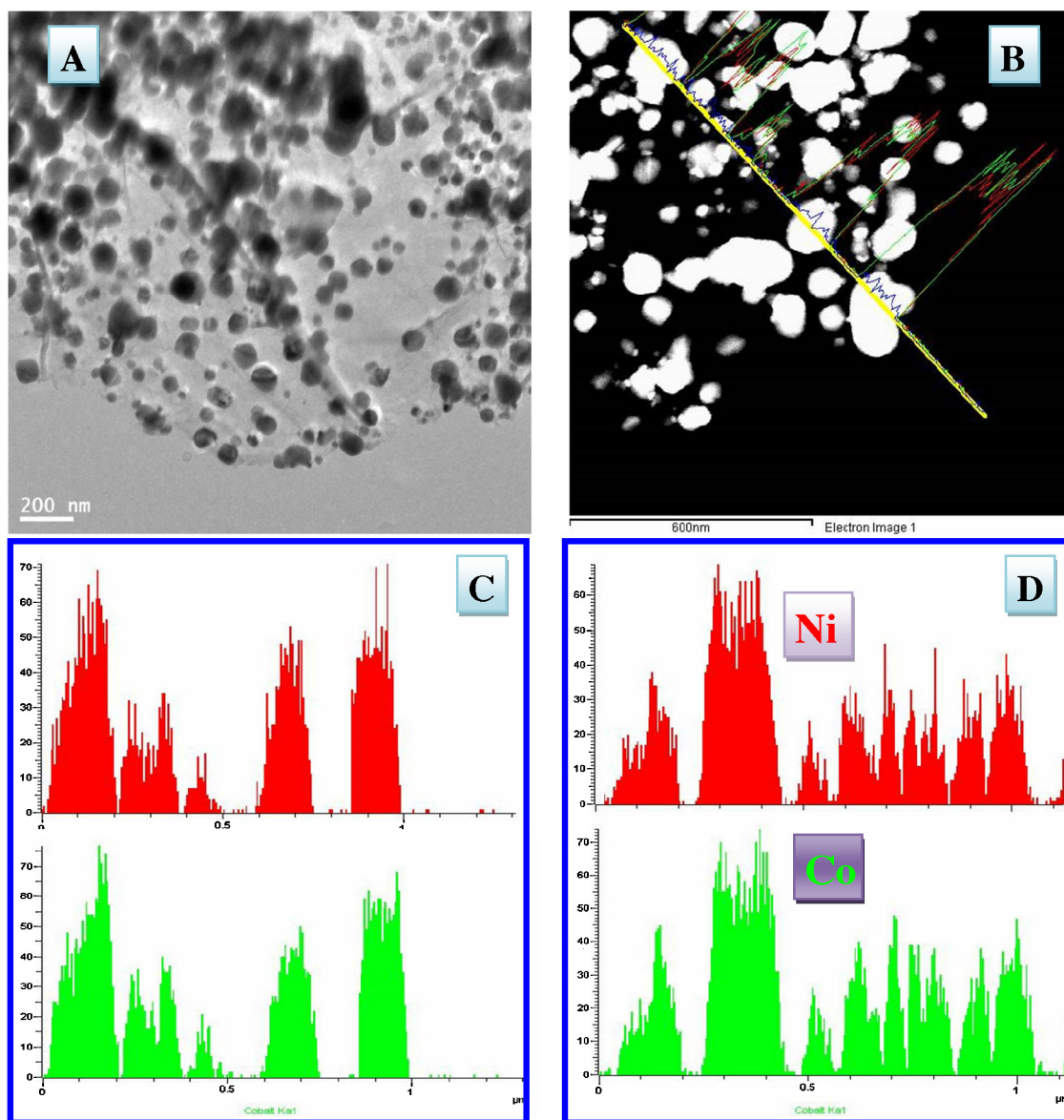


Fig. 4. TEM; (A) and linear TEM-EDX analyses at three different randomly chosen lines; (B), (C) and (D)..

hypothesis about formation of NiCo alloy nanoparticles attached with graphene sheets and simultaneously supports the XRD results.

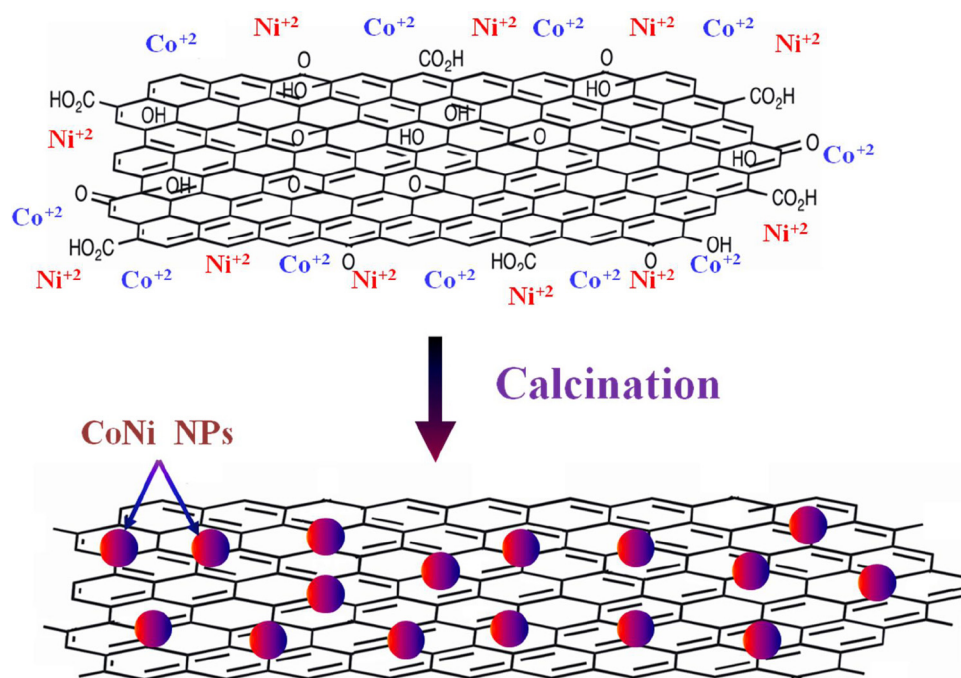
Attraction of the positively-charged metal ions by the polarised bonds of the functional groups on the GO is an accepted mechanism for the synthesis of inorganic nanostructures decorated graphene [42]. Accordingly, it can be claimed that during the reflux step, Co^{+2} and Ni^{+2} ions attached to the GO surface which resulted in formation of CoNi NPs during the calcination process. Scheme 1 displays conceptual illustration for the preparation mechanism.

The superior electrical conductivity and the huge specific surface area of graphene can have strong impacts on the electrochemical reactions of methanol oxidation. To properly investigate this hypothesis, the electro-catalytic activity of pristine nickel nanoparticles (Ni NPs, <25 nm, Aldrich) as a standard catalyst was compared to Ni-decorated graphene prepared by the same aforementioned procedure (the initial precursors were GO 300 mg and NiAc 400 mg); Fig. 5. As shown in the figure, supporting the Ni NPs on graphene sheets led to strong improvement for the electro-catalytic activity as the current density increased to 10 times. The distinct observed increase in the current density can be attributed

to the adsorption capacity of graphene which leads to bring the methanol molecules and the intermediates to the catalyst surface; moreover the high electrical conductivity of the support might contribute by fast removing for the liberating electrons. As it is expected, pristine graphene has almost no catalytic activity toward methanol oxidation as shown in the figure.

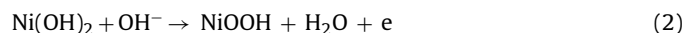
It is known that the alloy composition strongly affects the physicochemical characteristics. Fig. 6 displays the influence of the composition of the metallic NPs on the electro-catalytic activity. The loading weight was kept as 400 mg (NiAc + CoAc) per 300 mg GO. As shown in the figure, $\text{Co}_{0.2}\text{Ni}_{0.2}$ -decorated graphene revealed the best performance.

There are different mechanisms describing the heterogeneous catalysis. However, all the mechanisms agreed that the first step is adsorption of the reactant(s) on the active sites in catalyst surface. Later on, the bonds within the reacting molecules are weakened, and new bonds between the resulting fragments form in part due to their close proximity. In nickel based electro-catalysts, it is known that the catalyst has to be activated first by formation of NiOOH compound on the surface using cyclic voltammetry process in an



Scheme 1. Conceptual illustration for the CoNi-decorated synthesis mechanism.

alkaline media for many successive cycles [26]. Accordingly, anodic and cathodic peaks are observed in the activation voltammograms of the introduced decorated graphene electro-catalysts (Fig. 7). Typically, formation of the NiOOH layer was explained by the following reactions [26,43,44].



Increasing the number of potential sweeps results in a progressive increase of the current density values of the cathodic peak because of the entry of OH^- into the $\text{Ni}(\text{OH})_2$ surface layer, which leads to the progressive formation of a thicker NiOOH layer corresponding to the $\text{Ni}(\text{OH})_2/\text{NiOOH}$ transition which results in high catalytic activity [26]. There are some important information can be obtained from activation of the introduced decorated graphene.

The sample revealing the best performance ($\text{Co}_{0.2}\text{Ni}_{0.2}$ -decorated; Fig. 7C) has the maximum current densities in both of the cathodic and anodic peaks which might be the reason behind the corresponding highest electro-catalytic activity.

Excluding the best sample, in the other formulations, the current densities increase with increasing the potential sweeps which matches the nickel-based electro-catalysts.

Although other reports concluded that pristine cobalt has negligible electro-catalytic activity due to difficulties of surface activation [45,46], Co-decorated graphene could be activated which results in good performance as shown in Fig. 6.

For proper comparison, Fig. 8 which displays the 25th cycle in each formulation was established. Interestingly, the sequence in the current densities in both anodic and cathodic peaks matches the observed performance in Fig. 6. In other words, in both figures the order of the sample according to the corresponding current

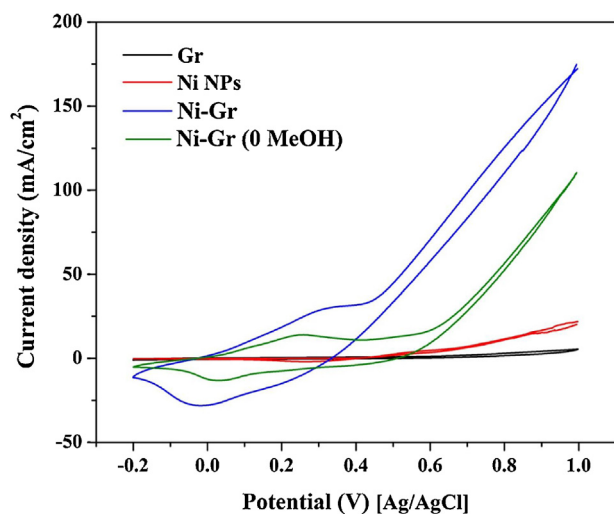


Fig. 5. Cyclic voltammograms at a scan rate of 50 mV/s and 25 °C for Ni NPs, pristine graphene and Ni-decorated graphene in 1 M KOH and in presence of 0.0 (for Ni-Gr only) and 3.0 M methanol.

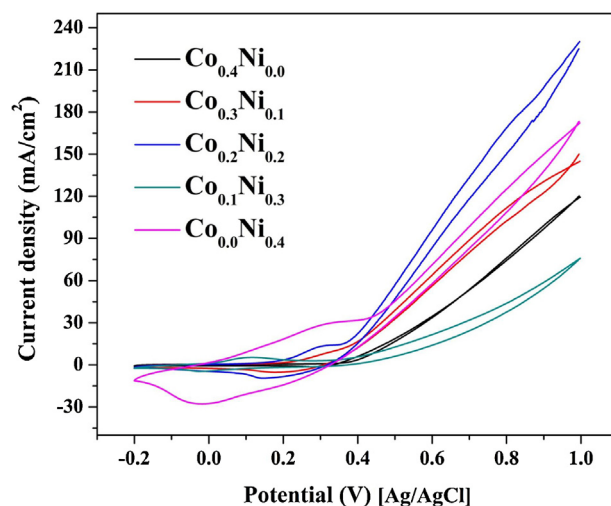


Fig. 6. Cyclic voltammograms at a scan rate of 50 mV/s and 25 °C for CoNi-decorated graphene with different concentrations for the metallic nanoparticles in 3 M methanol (in 1 M KOH)..

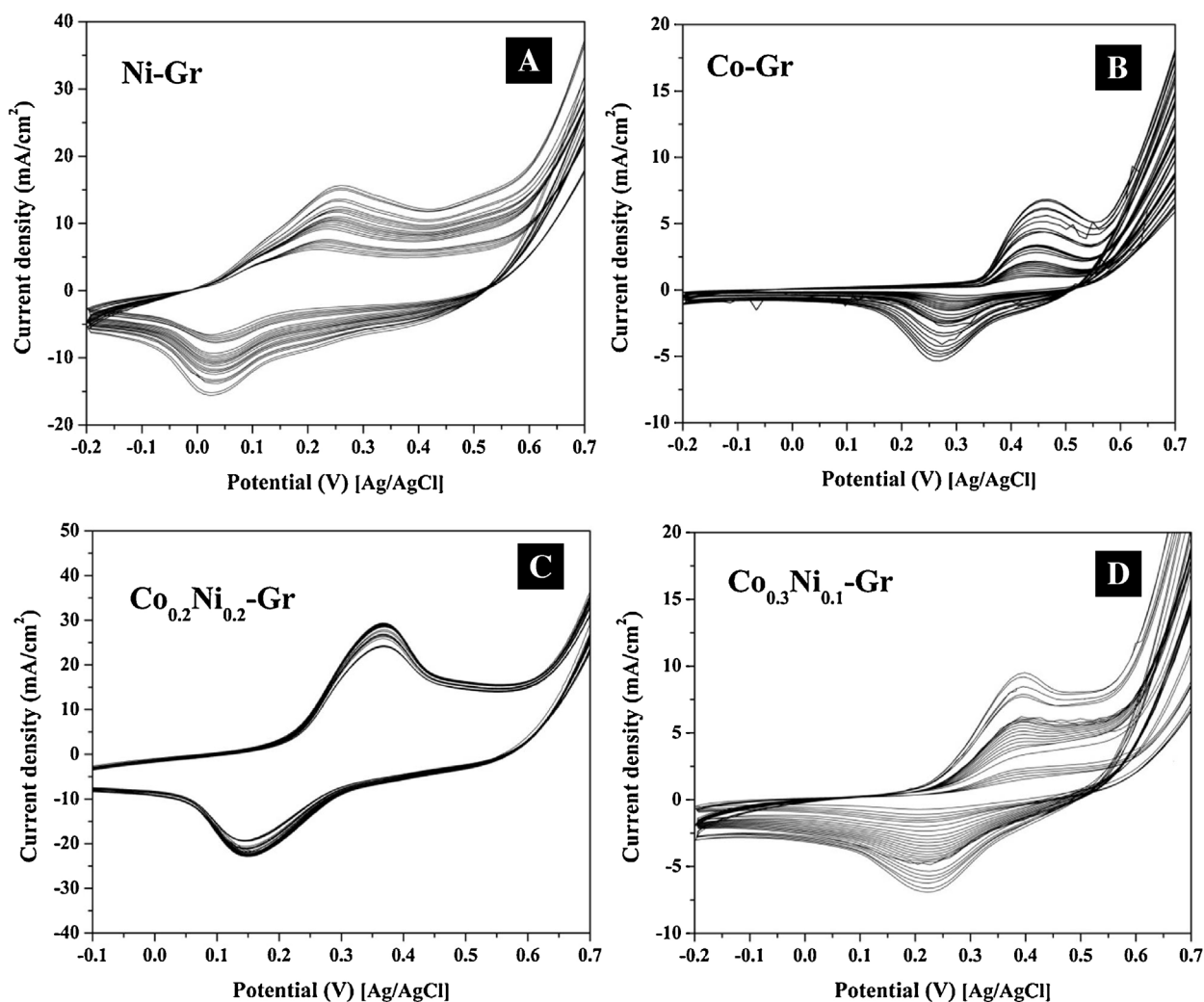


Fig. 7. Cyclic voltammograms in presence of 1 M KOH (scan rate 100 mV/s) for the introduced decorated graphene samples; Ni-decorated graphene; (A), Co-decorated graphene; (B), $\text{Co}_{0.2}\text{Ni}_{0.2}$ -decorated graphene; (C), and $\text{Co}_{0.3}\text{Ni}_{0.1}$ -decorated graphene; (D).

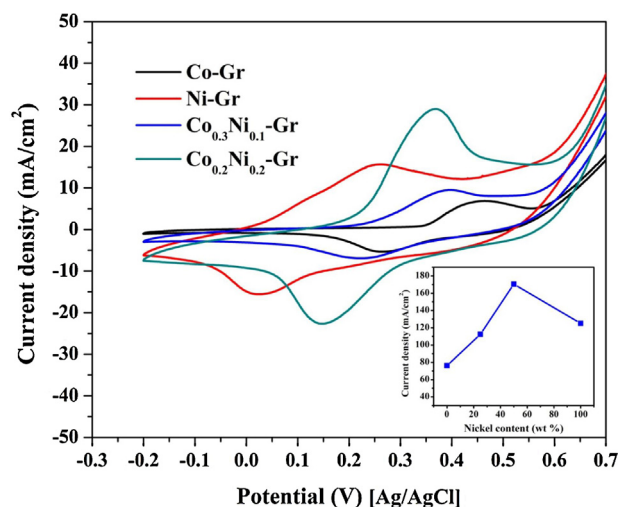


Fig. 8. Cyclic voltammograms for the 25th cycle during the activation process in presence of 1 M KOH (scan rate 100 mV/s) for the prepared decorated graphene samples. The inset displays relationship between the nickel content in the introduced decorated graphene and the current densities (at 0.8 V vs. Ag/AgCl) in presence of 3 M methanol.

densities is $\text{Co}_{0.2}\text{Ni}_{0.2}$ > Ni > $\text{Co}_{0.3}\text{Ni}_{0.1}$ > Co-decorated graphene. The inset in Fig. 8 represents the relationship between the anodic current density (at 0.8 V) and Ni content in the sample in presence of 3 M methanol.

The adsorption process and the catalytic activity mainly depend on the surface electronic structure which is responsible about creating the active sites on the catalysts surface. Of course, in alloys, the electronic structure is a composition-dependent variable. Therefore, one can claim that the electronic structure of $\text{Co}_{0.2}\text{Ni}_{0.2}$ alloy nanoparticle strongly enhances formation of the NiOOH active layer. Therefore, maximum amount of NiOOH was formed from almost the first cycle in the activation process (Fig. 7C). On the other hand, the electronic structure of $\text{Co}_{0.1}\text{Ni}_{0.3}$ alloy nanoparticle has negative impact on NiOOH formation, so the $\text{Co}_{0.1}\text{Ni}_{0.3}$ -decorated graphene revealed the worst performance among the prepared electro-catalysts (Fig. 6), even lower than Co-decorated graphene. It is noteworthy mentioning that almost no peaks were obtained during activation of this sample, data are not shown.

Fig. 9A represents the influence of the metallic nanoparticle loading for alloys having equal amounts from the two metals on the electro-catalytic activity. As shown in the figure, the graphene decorated by $\text{Ni}_{0.2}\text{Co}_{0.2}$ alloy NPs reveal the best performance among the utilized samples. For the sample having higher loading ($\text{Ni}_{0.4}\text{Co}_{0.4}$ -decorated graphene), it can be claimed that the comparatively low performance attributes to hiding more surface from the

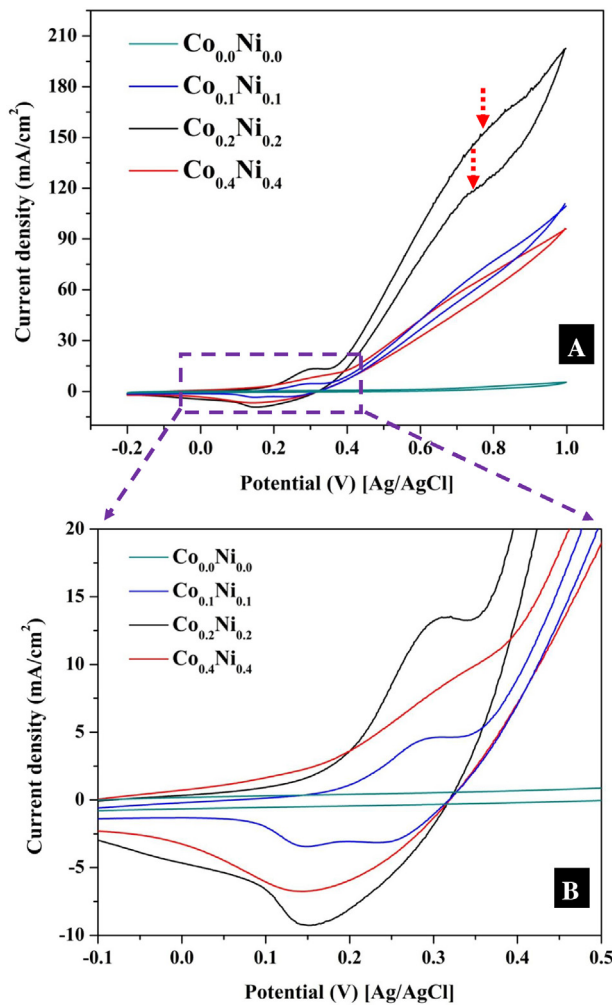


Fig. 9. (A) Cyclic voltammograms at a scan rate of 50 mV/s and 25 °C for CoNi-decorated graphene with different loading for the metallic nanoparticles in 3 M methanol (in 1 M KOH). (B) panel displays a high magnification for the marked area in panel A..

graphene sheet as shown in the TEM image of this sample (Fig. S3 in the supporting information). In other words, one can say that graphene adsorption capacity has a distinct role in the electro-oxidation process as graphene can adsorb the alcohols molecules and/or the reactions intermediates to complete the oxidation process. The electro-catalytic oxidation of methanol occurs not only in

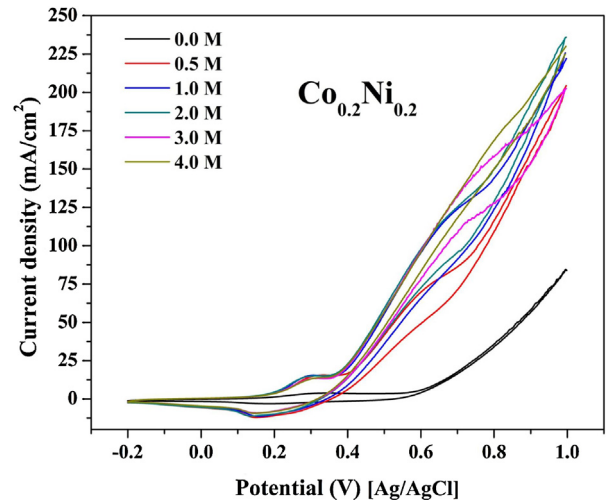


Fig. 10. Cyclic voltammograms at a scan rate of 50 mV/s and 25 °C for Co_{0.2}Ni_{0.2}-decorated graphene sample with different methanol concentrations (in 1 M KOH)..

the anodic but also continues in the initial stage of the cathodic half cycle. Methanol molecules adsorbed on the surface are oxidized at higher potentials parallel to the oxidation of Ni(II) to Ni(III) species. The later process has the consequence of decreasing the number of sites for methanol adsorption that along with the poisoning effect of the products or intermediates of the reaction tends to decrease the overall rate of methanol oxidation. Thus, the anodic current passes through a maximum as the potential is anodically swept. In the reverse half cycle, the oxidation continues and its corresponding current goes through the maximum due to the regeneration of active sites for adsorption of methanol as a result of the removal of adsorbed intermediates and products [31]. As shown in the lower panel (Fig. 9B), Co_{0.2}Ni_{0.2}-decorated graphene shows the minimum cathodic current. The arrows in Fig. 9A points to the methanol main oxidation peaks which clearly appear in case of the Co_{0.2}Ni_{0.2}-decorated graphene, however for the other formulation these peaks might appear at high voltage.

Utilizing highly concentrated alcohol solution in the DAFCs is strongly preferable because it distinctly diminishes the cells size and simultaneously improves the power density. Theoretically, using absolute methanol is not possible as water is a reactant in the anode reactions, so the alcohol concentration is a process parameter for the electro-catalysts. Beyond the concentration threshold the performance decreases. Fig. 10 displays the influence of methanol concentration on the electro-catalytic activity of Ni_{0.2}Co_{0.2}-decorated graphene. As shown in the figure, the

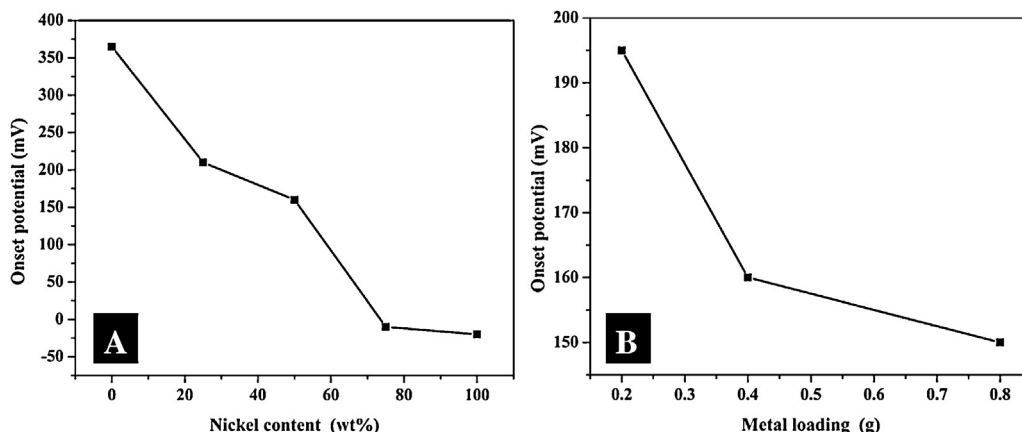


Fig. 11. Effect of nickel content; (A) and metal loading; (B) on the onset potential [vs. Ag/AgCl] of methanol oxidation (3 M) by the introduced decorated graphene.

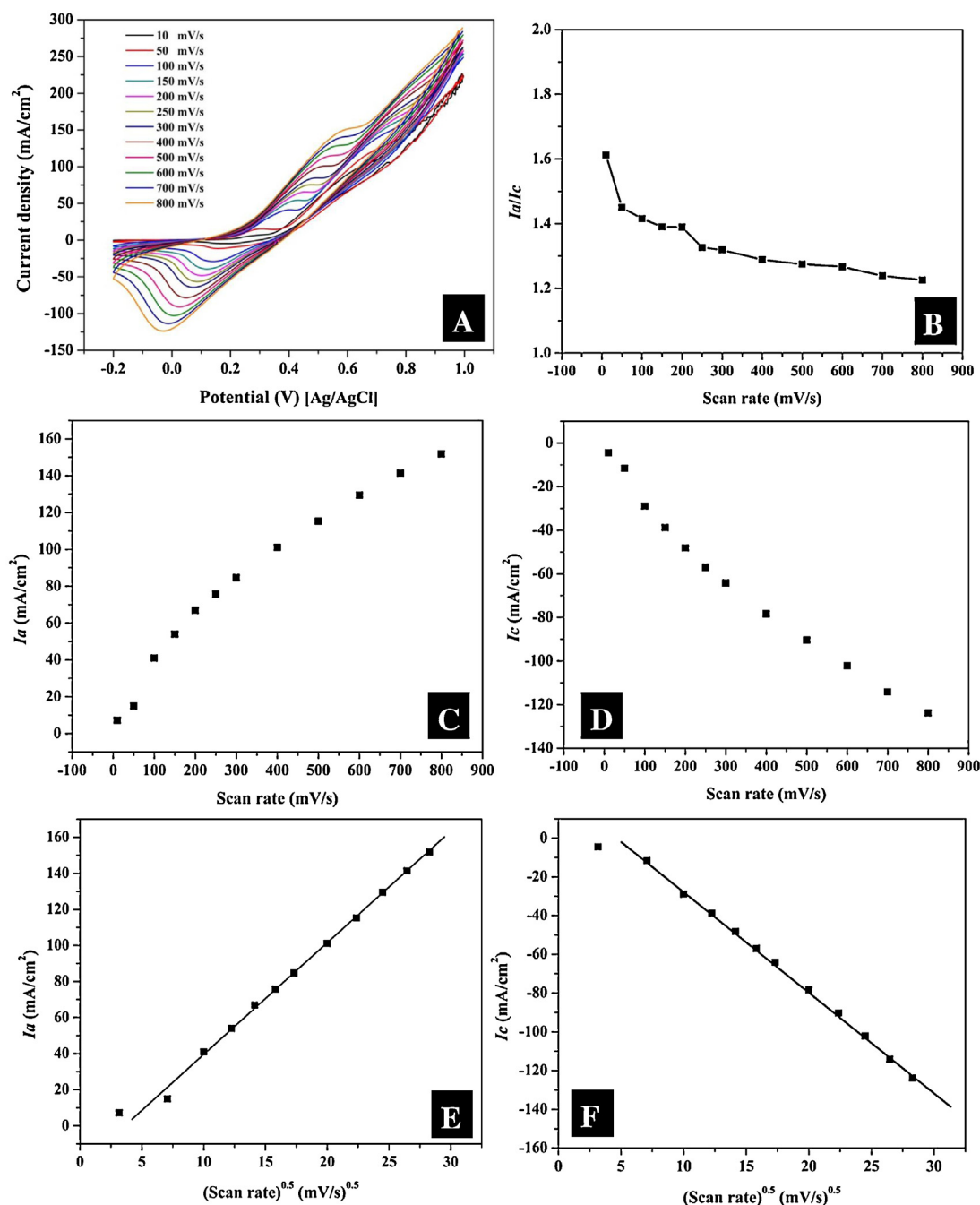


Fig. 12. Panel A shows the cyclic voltammograms at different scan rates for $\text{Ni}_{0.2}\text{Co}_{0.2}$ -decorated graphene sample in 1 M MeOH at 25 °C, B displays the relationship between the anodic (I_a) and cathodic (I_c) ratio, and the scan rate, C and D display the variation of I_a and I_c with the scan rate, respectively, and E and F show the relationship between the I_a and I_c peaks current and the square root of the scan rates, respectively.

concentration can be increased to 4 M methanol. This is an interesting finding as the sample giving the best performance in all investigations ($\text{Ni}_{0.2}\text{Co}_{0.2}$ -decorated graphene) can be exploited with relatively high concentrated methanol solution. Fig. S.4 in the supporting information displays the influence of methanol concentration on the electro-catalytic activities of other samples.

Among the invoked parameters to demonstrate the electro-catalytic activity, the onset potential which indicates the electrode overpotential has special consideration. The efficacy of the electro-catalyst can be evaluated from the onset potential. In alcohol electro-oxidation, high activity and less overpotential corresponds to more negative onset potential. In case of Pt-based catalysts, adsorption of OH and CO adsorbed is the main reason behind

increasing the onset potential [47], however small organic molecules are usually not fully oxidized and adsorbed on the surface of nickel-based materials [48]. The small value of the corresponding onset potentials is one important advantage for the Pt-based electrodes over the non-precious electro-catalysts. Fig. 11A represents the effect of nickel content on the onset potential of the introduced decorated graphene electro-catalysts. Interestingly, utilizing of graphene as a supporter for the nickel nanoparticles led to have a negative onset potential of -40 mV (vs. Ag/AgCl). It is noteworthy mentioning that the unsupported Ni NPs reveal onset potential of ~ 490 mV [vs. Ag/AgCl RE]; Fig. 5. To properly demonstrate the onset potential of the introduced decorated graphene as well as correctly estimate the onset potential [49], the

CV cycle for Ni-Gr electrode in absence of methanol (only 1 M KOH) was added to Fig. 5, as shown methanol starts to be oxidized at relatively very low voltage. This is a very promising result as according to our best knowledge, for the non-precious electro-catalysts, it is the lowest onset potential value reported in the literature so far. Concerning $\text{Ni}_{0.2}\text{Co}_{0.2}$ -decorated graphene sample, it has a corresponding onset potential of 160 mV [vs. Ag/AgCl] which is also small compared to many reported non-precious electro-catalysts. Fig. 11B shows the change in the onset potential with the metallic particles loading, as can be concluded from the figure increase the loading leads to a slight decrease in the onset potential.

For the catalytic reactions, the concept of the rate-determining step is very important to the optimization and understanding of the process. The rate of a reaction mechanism with several steps is often determined by the slowest step, known as the rate-determining step. Fig. 12A displays the cyclic voltammograms for the sample showing the best performance ($\text{Ni}_{0.2}\text{Co}_{0.2}$ -decorated graphene) at different scan rates in 3 M methanol solution. As shown in the figure, increasing the scan rate causes increase the intensities of the cathodic and anodic peaks. The current ratio of the oxidation–reduction peaks ($I_a:I_c$) at different scan rates are shown in Fig. 12B. At the low scan rates, the ratio is not low which indicates fast formation of NiOOH layers compared to $\text{Ni}(\text{OH})_2$, however within this small range the ratio is not very high (from 1.6 to ~ 1.2) which indicates good reversibility. After scan rate value of 250 mV/s, almost no change in the $I_a:I_c$ ratio is observed as shown in the figure with small corresponding value; ~ 1.2 .

The surface coverage of the redox species in mol cm^{-2} Γ can be estimated from the following equation [50]

$$I_p = \left(\frac{n^2 F^2}{4RT} \right) \nu A \Gamma \quad (3)$$

where I_p is the peak current, n is the number of electrons sharing in the reaction, ν is the scan rate and A is the electrode area. Fig. 12C and D displays the effect of the scan rate on the anodic and cathodic peaks current, respectively. From the slopes of the straight lines representing these data points, the surface coverage can be determined. Taking average of both cathodic and anodic results, values of around $3.05 \times 10^{-7} \text{ mol/cm}^2$ have been derived that correspond to the presence of around 250 monolayers of surface species for the $\text{Co}_{0.2}\text{Ni}_{0.2}$ -decorated graphene electrode. Fig. 12E and F shows the relationships between the anodic and cathodic currents, respectively and the square root of the scan rates to determine the rate controlling step. High accuracy linear models could be utilized to represent the data points. This finding signifies the dominance of the diffusion controlled processes which indicates high activity of the introduced electro-catalyst [50].

Fig. 13A displays the cyclic voltammograms for the best sample ($\text{Co}_{0.2}\text{Ni}_{0.2}$ -loaded graphene) for some randomly selected cycles from 250 total cycles. As shown in the figure, good stability can be observed. It is acceptable to say that the alloy structure is the main reason behind the good stability obtained. Fig. 13B displays the chronoamperograms which were recorded on $\text{Co}_{0.2}\text{Ni}_{0.2}$ -Gr electrode for 1000 min at 0.20 and 0.40 V potentials in 3.0 M $\text{CH}_3\text{OH} + 1.00 \text{ M KOH}$. As time progresses, methanol oxidation current slightly decreases and then remains constant. At first, the active sites are free of adsorbed methanol molecules (fast kinetic rate reaction); after that the adsorption of new methanol molecules is a function of the liberation of the active sites by methanol oxidation or intermediate species formed during the first minutes (rate determining step) [51] that are responsible for poisoning of the catalytic sites. The result indicates that the investigated electrode exhibits distinct stability.

Electrochemical impedance spectroscopy (EIS) was performed on the Gr, Co-Gr, Ni-Gr and $\text{Co}_{0.2}\text{Ni}_{0.2}$ -Gr electrodes to properly

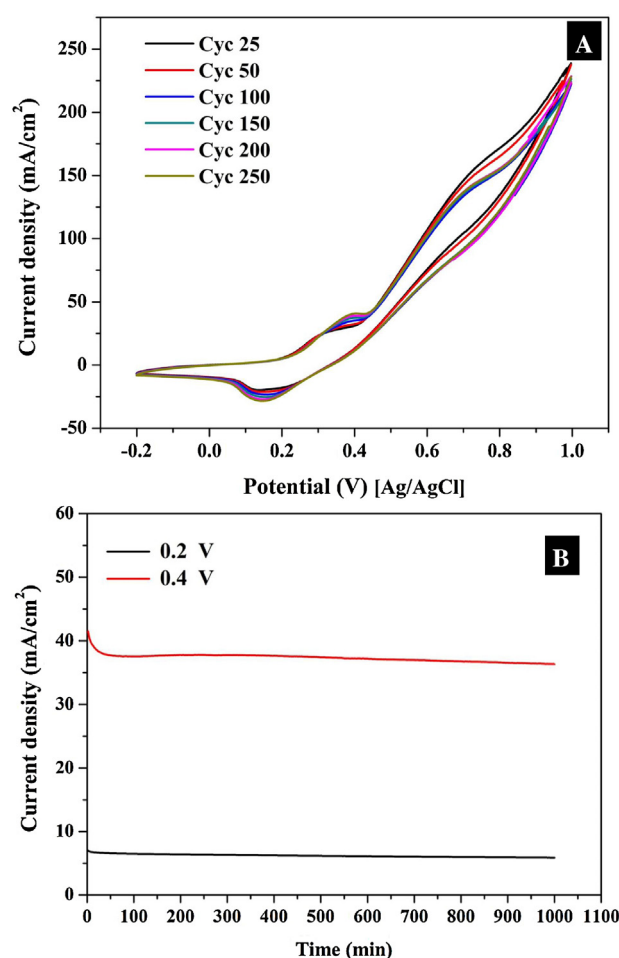


Fig. 13. Cyclic voltammograms for randomly selected cycles (scan rate of 50 mV/s and 25 °C, 3 M methanol); (A), and chronoamperometry at 0.2 and 0.4 V; (b) for $\text{Co}_{0.2}\text{Ni}_{0.2}$ -decorated graphene sample.

investigate the methanol oxidation. Nyquist plots for the investigated electrodes in different methanol concentrations (0, 1, 2 and 3 M + 1.0 M KOH) are displayed in Fig. 14. Fig. 14A represents the Nyquist plot of the pristine graphene electrode, the obtained plot indicates that the electrode cells do not have Faradaic reactions, current leads to capacitive charging of the double layers. In other words, it can be concluded that the cell has polarizable electrodes, this hypothesis is confirmed by the negligible influence of increasing methanol concentration on the Nyquist plots as shown in the figure and the corresponding inset. This finding supports the very low electrocatalytic activity of graphene toward methanol oxidation. In the Nyquist plot, the Faradaic reaction (methanol oxidation) usually displayed by capacitive loop with a diameter almost matching the charge transfer resistance (R_{CT}). Fig. 14B, C and D displays the Nyquist plots for Co-Gr, Ni-Gr and $\text{Co}_{0.2}\text{Ni}_{0.2}$ -Gr, respectively as shown in this figure the capacitive loops appear when methanol was present in the electrolyte solutions which clearly indicates the electrocatalytic activity of these electrodes. Table 1 summarizes the values of the R_{CT} in $\Omega \text{ cm}^2$ for the investigated electrodes at different methanol concentrations. As shown in the table, compared to Ni-Gr and Co-Gr, the introduced bimetallic alloy reveals lower charge transfer resistance which indicates higher electrocatalytic activity. It is noteworthy mentioning that low charge transfer resistance demonstrates fast electron-transfer rate on the electrocatalyst [52].

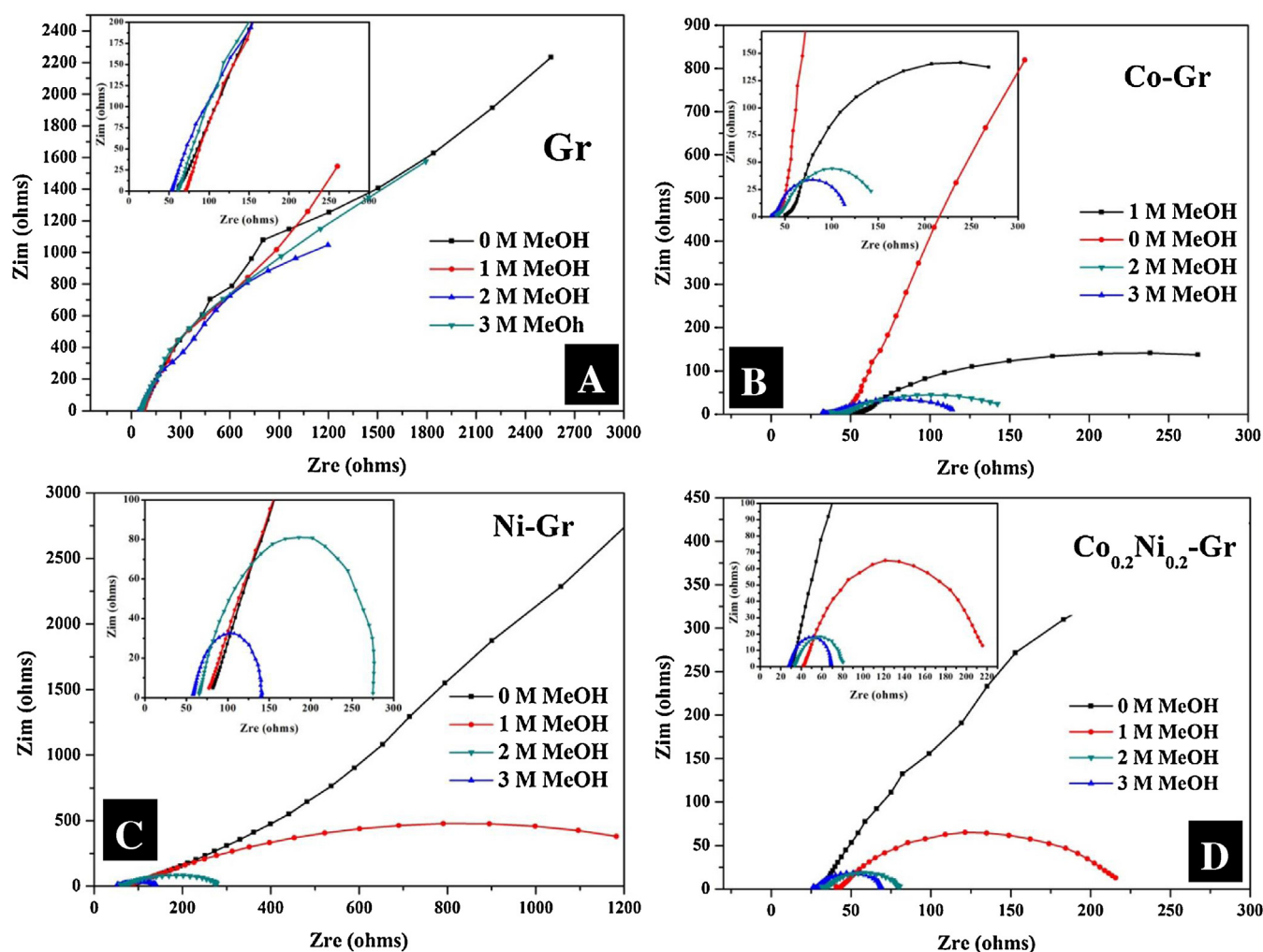


Fig. 14. Nyquist plots for the oxidation reaction at 0.60 V on Gr; (A), Co-Gr; (B), Ni-Gr; (C), and $\text{Co}_{0.2}\text{Ni}_{0.2}\text{-Gr}$; (D).

Table 1

Charge transfer resistance (R_{CT} , Ωcm^2) for the utilized electrodes at different methanol concentrations.

Electrode	Methanol concentration (M)			
	0.0	1.0	2.0	3.0
Co-Gr	–	–	6.601	5.128
Ni-Gr	–	–	14.595	5.788
$\text{Co}_{0.2}\text{Ni}_{0.2}\text{-Gr}$	–	12.0932	3.168	2.824

4. Conclusion

Good chemical corrosion resistance and high electro-catalytic activity toward methanol electro-oxidation can be obtained from CoNi-decorated graphene. The proposed electro-catalyst can be produced by adding cobalt acetate and nickel acetate in the reaction media during graphene preparation using the chemical route. Calcination of the resultant decorated graphene in argon atmosphere is an important step to produce solid solution CoNi alloy nanoparticle. Due to the super electric conductivity and excellent adsorption capacity, utilizing graphene as a supporter strongly enhances the electro-catalytic activity toward methanol oxidation. The composition and the loading of the alloy nanoparticle have a distinct influence on electro-catalytic activity; $\text{Ni}_{0.2}\text{Co}_{0.2}$ -decorated graphene reveals the best results. The introduced electro-catalyst has good stability in the alkaline media because of the alloy structure.

Appendix A. Supplementary data

Supplementary material related to this article can be found, in the online version, at <http://dx.doi.org/10.1016/j.apcatb.2014.02.019>.

References

- [1] Y. Chu, Y. Shul, Fuel Cells 12 (2012) 109–115.
- [2] M.Z.F. Kamarudin, S.K. Kamarudin, M.S. Masdar, W.R.W. Daud, Int. J. Hydrogen Energy 38 (2013) 9438–9453.
- [3] J. Prakash, D.A. Tryk, E.B. Yeager, J. Electrochem. Soc. 146 (1999) 4145–4151.
- [4] Y.G. Guo, J.S. Hu, L.J. Wan, Adv. Mater. 20 (2008) 2878–2887.
- [5] J. Shen, Y. Hu, C. Li, C. Qin, M. Ye, Electrochim. Acta 53 (2008) 7276–7280.
- [6] N. Hampson, M. Willars, B. McNicol, J. Power Sources 4 (1979) 191–201.
- [7] H.A. Gasteiger, N. Markovic, P.N. Ross Jr., E.J. Cairns, J. Phys. Chem. 97 (1993) 12020–12029.
- [8] C. Wang, M. Waje, X. Wang, J.M. Tang, R.C. Haddon, Y. Yan, Nano Lett. 4 (2004) 345–348.
- [9] W. Li, C. Liang, J. Qiu, W. Zhou, H. Han, Z. Wei, G. Sun, Q. Xin, Carbon 40 (2002) 787–790.
- [10] W. Li, C. Liang, W. Zhou, J. Qiu, Z. Zhou, G. Sun, Q. Xin, J. Phys. Chem. B 107 (2003) 6292–6299.
- [11] E.S. Steigerwalt, G.A. Deluga, D.E. Cliffel, C. Lukehart, J. Phys. Chem. B 105 (2001) 8097–8101.
- [12] Y. Lu, R.G. Reddy, Int. J. Hydrogen Energy 33 (2008) 3930–3937.
- [13] A.K. Geim, K.S. Novoselov, Nat. Mater. 6 (2007) 183–191.
- [14] L. Rodríguez-Pérez, M.A. Herranz, N. Martín, Chem. Commun. 49 (2013) 3721–3735.
- [15] A. Peigney, C. Laurent, E. Flahaut, R. Bacs, A. Rousset, Carbon 39 (2001) 507–514.
- [16] N. Savage, Nature 483 (2012) S30–S31.

- [17] Y. Mu, H. Liang, J. Hu, L. Jiang, L. Wan, *J. Phys. Chem. B* 109 (2005) 22212–22216.
- [18] W. Li, W. Zhou, H. Li, Z. Zhou, B. Zhou, G. Sun, Q. Xin, *Electrochim. Acta* 49 (2004) 1045–1055.
- [19] E. Yoo, T. Okata, T. Akita, M. Kohyama, J. Nakamura, I. Honma, *Nano Lett.* 9 (2009) 2255–2259.
- [20] Y.-G. Zhou, J.-J. Chen, F.-b. Wang, Z.-H. Sheng, X.-H. Xia, *Chem. Commun.* 46 (2010) 5951–5953.
- [21] Y. Li, W. Gao, L. Ci, C. Wang, P.M. Ajayan, *Carbon* 48 (2010) 1124–1130.
- [22] R. Awasthi, R.N. Singh, *Carbon* 51 (2013) 282–289.
- [23] S.M. Choi, M.H. Seo, H.J. Kim, W.B. Kim, *Carbon* 49 (2011) 904–909.
- [24] C.H. Yen, K. Shimizu, Y.Y. Lin, F. Bailey, I.F. Cheng, C.M. Wai, *Energy Fuels* 21 (2007) 2268–2271.
- [25] E. Frackowiak, G. Lota, T. Cacciaguerra, F. Béguin, *Electrochem. Commun.* 8 (2006) 129–132.
- [26] A. Rahim, R. Abdel Hameed, M. Khalil, *J. Power Sources* 134 (2004) 160–169.
- [27] C. Fan, D. Piron, A. Sleb, P. Paradis, *J. Electrochem. Soc.* 141 (1994) 382–387.
- [28] I.A. Raj, K. Vasu, *J. Appl. Electrochem.* 20 (1990) 32–38.
- [29] J.M. Marioli, P.F. Luo, T. Kuwana, *Anal. Chim. Acta* 282 (1993) 571–580.
- [30] J.M. Marioli, T. Kuwana, *Electroanalysis* 5 (1993) 11–15.
- [31] I. Danaee, M. Jafarian, A. Mirzapoor, F. Gopal, M. Mahjani, *Electrochim. Acta* 55 (2010) 2093–2100.
- [32] F.A. Sheikh, J. Macossay, M.A. Kanjwal, A. Abdal-hay, M.A. Tantry, H. Kim, *ISRN Nanomater.* 2012 (2012).
- [33] U. Paulus, A. Wokaun, G. Scherer, T. Schmidt, V. Stamenkovic, V. Radmilovic, N. Markovic, P. Ross, *J. Phys. Chem. B* 106 (2002) 4181–4191.
- [34] Y. Xu, H. Bai, G. Lu, C. Li, G. Shi, *JACS* 130 (2008) 5856–5857.
- [35] W.S. Hummers Jr., R.E. Offeman, *JACS* 80 (1958) 1339.
- [36] S. Stankovich, D.A. Dikin, R.D. Piner, K.A. Kohlhaas, A. Kleinhammes, Y. Jia, Y. Wu, S.B.T. Nguyen, R.S. Ruoff, *Carbon* 45 (2007) 1558–1565.
- [37] Y. Zhu, S. Murali, W. Cai, X. Li, J.W. Suk, J.R. Potts, R.S. Ruoff, *Adv. Mater.* 22 (2010) 3906–3924.
- [38] S. Stankovich, R.D. Piner, X. Chen, N. Wu, S.T. Nguyen, R.S. Ruoff, *J. Mater. Chem.* 16 (2006) 155–158.
- [39] C.F. Chang, Q.D. Truong, J.R. Chen, *Appl. Surf. Sci.* 264 (2013) 329–334.
- [40] A.B. Bourlinos, D. Gournis, D. Petridis, T. Szabó, A. Szeri, I. Dékány, *Langmuir* 19 (2003) 6050–6055.
- [41] F. Tuinstra, J. Koenig, *J. Compos. Mater.* 4 (1970) 492–499.
- [42] P.S. Teo, H.N. Lim, N.M. Huang, C.H. Chia, I. Harrison, *Ceram. Int.* 38 (2013) 6411–6416.
- [43] F. Hahn, B. Beden, M. Croissant, C. Lamy, *Electrochim. Acta* 31 (1986) 335–342.
- [44] M. Vuković, *J. Appl. Electrochem.* 24 (1994) 878–882.
- [45] N.A. Barakat, M.A. Abdelkareem, H.Y. Kim, *Appl. Catal. A* 455 (2013) 193–198.
- [46] N.A.M. Barakat, M.A. Abdelkareem, A. Yousef, S.S. Al-Deyab, M. El-Newehy, H.Y. Kim, *Int. J. Hydrogen Energy* 38 (2013) 3387–3394.
- [47] D. Geng, G. Lu, *J. Phys. Chem. C* 111 (2007) 11897–11902.
- [48] M. Fleischmann, K. Korinek, D. Pletcher, *J. Electroanal. Chem. Interfacial Electrochem.* 31 (1971) 39–49.
- [49] M. Sattar, B. Conway, *Electrochim. Acta* 14 (1969) 695–710.
- [50] A. Bard, L. Faulkner, *Electrochemical Methods*, Wiley, New York, 2001 (Chapter 12).
- [51] E. Antolini, *Appl. Catal. B* 74 (2007) 337–350.
- [52] A. Döner, E. Telli, G. Kardaş, *J. Power Sources* 205 (2012) 71–79.